

## Shear wave propagation in jointed rock: state of stress

D. FRATTA\* and J. C. SANTAMARINA†

The mechanical characteristics and orientation of joints determine the behaviour of rock masses, including the strength, the stiffness, and all forms of conduction and diffusion. Furthermore, the preferential orientation of joints renders the medium anisotropic. In turn, these properties affect the velocity and damping of propagating elastic waves. The purpose of this study is to investigate the propagation of long-wavelength shear waves through a rock mass with open joints filled with softer gouge, and subjected to low confinement. These conditions are selected in view of near-surface geophysical characterisation studies for geotechnical engineering applications such as foundations, tunnels and slopes. Experimental data are gathered with a slender column made of discrete elements with gouge material in the joints. The column is excited in the first torsional vibration mode to gather accurate measurements of velocity and damping for wave propagation direction normal to the joints. Data are analysed with mixture models. The potential use of wave propagation methods to assess jointed rock masses is discussed.

**KEYWORDS:** dynamics; elasticity; laboratory tests; site investigations; rocks/rock mechanics; stiffness; waves and wave loading

Les caractéristiques mécaniques et l'orientation des joints déterminent le comportement des masses rocheuses, notamment la longueur, la rigidité et toutes les formes de conduction et de diffusion. De plus, l'orientation préférentielle des joints rend le milieu anisotrope. Pour leur part, ces propriétés affectent la vitesse et l'amortissement des ondes élastiques qui se propagent. Cette étude a pour but d'examiner la propagation des ondes de cisaillement ayant une grande longueur d'onde à travers une masse rocheuse à joints ouverts remplis d'une glaise plus tendre et soumise à un faible confinement. Ces conditions sont choisies au regard d'études de caractérisation géophysique proche de la surface pour des applications d'ingénierie géotechnique telles que des tunnels, des fondations et des talus. Nous obtenons les données expérimentales à partir d'une colonne mince faite d'éléments discrets, avec glaise dans les joints. La colonne est excitée dans le premier mode de vibration à torsion afin de donner des mesures exactes de la vitesse et de l'amortissement pour une direction de propagation d'onde verticale aux joints. Nous analysons les données avec les modèles de mixture. Nous discutons de l'utilisation potentielle des méthodes de propagation des ondes pour évaluer les masses rocheuses fissurées.

### INTRODUCTION

The presence of joints and their characteristics determine the behaviour of the rock mass, including its strength, stiffness, and all forms of conduction and diffusion—hydraulic, electrical, chemical and thermal; if joints are preferentially orientated, the rock mass properties become anisotropic (Jumikis, 1983; Goodman, 1989; Guéguen and Palciauskas, 1994). The strength, stiffness and aperture of discontinuities depend on the stress level acting on the joint surfaces. In turn, these properties affect the velocity and damping of propagating elastic waves. These observations suggest the potential use of wave propagation methods to infer joint characteristics.

The building blocks for the understanding of wave propagation in jointed rock masses combine theoretical and experimental developments starting with Newton's study of sound propagation in discrete media and Fermat's understanding of travel path leading to reflection and refraction laws. The need for enhanced geophysical methods in oil exploration in the twentieth century and developments in seismology stimulated further progress on models for layered media, including the associated effects of anisotropy.

Dynamic analyses in geotechnical engineering and developments in high-resolution seismic methods for near-surface geotechnical characterisation raise new questions related to

wave propagation in jointed rock masses. Often, the operating frequency may be high, joints are subjected to low normal stress, and advanced weathering may have rendered filled joints. Robust analytical models with a limited number of variables could be used to infer rock mass parameters from wave propagation data. However, such models would require experimental validation. Unfortunately, the experimental study of long-wavelength propagation in jointed rock masses demands large specimens and high-capacity reaction frames.

This study is centred on shear wave propagation in jointed rocks, with and without gouge, subjected to low confinement. These choices respond to common conditions in the near surface and the need to characterise the skeletal stiffness of the jointed rock, rather than the bulk stiffness of saturating pore fluids. This study starts by analysing wave propagation in jointed rock masses. Then a set of unique experiments is conducted to assess the stress-dependent shear wave velocity and damping in a jointed rock mass. Finally, the dataset is analysed within the framework of analytical mixture models, taking into consideration the continuum nature of the blocks and the particulate nature of the gouge.

### WAVE PROPAGATION: OPEN JOINTS WITH GOUGE

The wavelength,  $\lambda$ , is the length scale of the propagating wave. The separation between joints is a salient length scale in the rock mass, herein called  $L_{\text{mass}} = L_r + L_j$ , where  $L_r$  is the thickness of the rock block,  $L_j$  is the aperture of the joint (Fig. 1), and the subscripts mass, r and j refer to the jointed rock mass, the intact rock block and the joint respectively. Therefore wave propagation in jointed rocks

Manuscript received 7 August 2001; revised manuscript accepted 7 May 2002.

Discussion on this paper closes 1 March 2003, for further details see p. ii.

\* Louisiana State University, Baton Rouge, USA.

† Georgia Institute of Technology, Atlanta, USA.

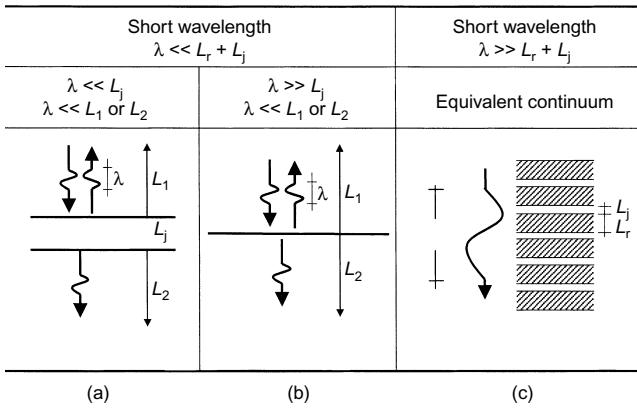


Fig. 1. Wave propagation in jointed media: short- and long-wavelength cases

can be organised into two extreme cases. The short-wavelength or high-frequency case takes place when the wavelength is much shorter than the separation between joints,  $\lambda \ll L_{mass}$ . The long-wavelength or low-frequency case applies when  $\lambda \gg L_{mass}$ .

Simple expressions for velocity and damping in rock masses with open joints filled with gouge are developed next. Both short- and long-wavelength propagation cases are considered. The particulate nature of the gouge is captured with semi-empirical relations for velocity and damping previously developed for soils.

Short wavelength ( $\lambda \ll L_{mass}$ )

A high-frequency, short-wavelength plane wave propagating normal to the layering traverses through each component as in an infinite medium, attenuating according to the material attenuation of the medium and experiencing partial transmission and reflection at interfaces. Both reflected and transmitted components generated at an interface experience subsequent reflections and transmissions at other interfaces. The transmitted wave experiences dispersion and attenuation.

If the joint is thick, wave propagation resembles a three-media problem: rock–joint–rock. The wave propagation velocity in the rock mass is determined from the cumulative travel time required to traverse the rock block and the joint:  $t_{mass} = t_r + t_j$ . The resulting expression for the short-wavelength wave velocity is a length-weighted average of the propagation velocities in the intact rock,  $V_r$ , and in the joint,  $V_j$ :

$$V_{mass}^{(short \lambda)} = \frac{L_{mass}}{\frac{L_r}{V_r} + \frac{L_j}{V_j}} = \frac{1}{\frac{1-\eta}{V_r} + \frac{\eta}{V_j}} \tag{1}$$

where  $\eta = L_j/L_{mass}$  is the joint ratio. This equation is known as *Wyllie's time-average* (Wyllie *et al.*, 1956).

The global attenuation combines the attenuation within each medium and the partial transmission that takes place at the joint:

$$e^{-\alpha_{mass} L_{mass}} = e^{-\alpha_j L_j} e^{-\alpha_r L_r} T \tag{2}$$

where  $T$  is the effective transmission coefficient across the joint, and attenuation coefficients  $\alpha_{mass}$ ,  $\alpha_j$  and  $\alpha_r$  correspond to the rock mass, the gouge material in the joint and the intact rock respectively. Therefore the attenuation in the rock mass for short-wavelength propagation is

$$\alpha_{mass}^{(short \lambda)} = \alpha_r(1 - \eta) + \alpha_j \eta - \frac{\ln T}{L_{mass}} \tag{3}$$

Assuming small losses, the attenuation coefficient in a medium can be related to the material damping,  $D$ , as

$$D = \frac{\alpha V}{2\pi f} \tag{4}$$

where  $V$  is the wave velocity and  $f$  is the frequency. Therefore equation (3) can be rewritten in terms of damping as

$$D_{mass}^{(short \lambda)} = D_r \frac{V_{mass}}{V_r} (1 - \eta) + D_j \frac{V_{mass}}{V_j} \eta - \frac{V_{mass}}{2\pi f L_{mass}} \ln T \tag{5}$$

The transmission coefficient,  $T$ , depends on the relative mechanical impedance between the rock blocks and the gouge, and on the ratio between the thickness of the joint,  $L_j$ , and the wavelength of the travelling wave within the gouge,  $\lambda = V/f$ . The three-media transmission coefficient without multiple reflections is (Brekhovskikh, 1960; Fig. 1(a))

$$T = \frac{4Z_r Z_j}{-(Z_r - Z_j)^2 \exp\left(i \frac{2\pi f}{V_j} L_j\right) + (Z_r + Z_j)^2 \exp\left(-i \frac{2\pi f}{V_j} L_j\right)} \tag{6}$$

where  $Z$  refers to the mechanical impedance of each medium,  $Z = \rho V$ ,  $\rho$  is the mass density, and  $i^2 = -1$  is the complex operator. If the joint thickness is very small compared with the wavelength ( $\lambda \gg L_j$ ) and with the length of the rock block ( $L_r \gg L_j$ , that is, the joint ratio approaches  $\eta = 0$ ), the contribution of  $D_j$  vanishes from equation (5), the transmission coefficient becomes  $T = 1.0$ , and the wave does not detect the presence of the joint. However, experimental data show that energy loss and time delay take place at joints, even in closed joints (Pyrak-Nolte *et al.*, 1990a, 1990b). Assuming the development of a displacement discontinuity at the joint—that is, stresses are continuous but displacements are not—the transmission coefficient is (Fig. 1(b); Pyrak-Nolte *et al.*, 1990a, 1990b; Boadu & Long, 1996)

$$T = 1 + \frac{j\omega}{\frac{2\kappa}{Z_r} - j\omega} \tag{7}$$

where the specific stiffness of the joint,  $\kappa$ , for a normally incident shear wave is the ratio between the shear stress applied and the displacement it produces parallel to the joint. The transmission coefficient from the displacement discontinuity model predicts that the time delay and the partial transmission across the joint are frequency dependent; in fact, the joint acts as a low-pass filter with cut-off frequency equal to  $2\kappa/Z_r$ .

The previous analysis considers only the first-pass signals, and disregards the multiple reflections and transmissions. Propagation in the short-wavelength regime can be modelled in the context of ray theory. In this case, effective numerical methodologies can be implemented to compute the transmitted signal recursively, taking into consideration all multiples (Mavko *et al.*, 1998).

Long wavelength ( $\lambda \gg L_{mass}$ )

When the wavelength,  $\lambda$ , is much larger than the separation between discontinuities,  $\lambda \gg L_{mass}$ , the medium can be analysed as an equivalent continuum with effective media properties (Fig. 1(c)). White (1983) recognises the localised deformation at interacting joint asperities and models the joint as Hertz–Mindlin contacts; the resulting rock mass

modulus is inherently stress-dependent. Alternatively, the displacement discontinuity hypothesis can be invoked, as in Pyrak-Nolte *et al.* (1990b). The long-wavelength propagation in directions not collinear with the joint pattern is captured with anisotropic material models (Postma, 1955; Crampin, 1977, 1984; Helbig, 1984).

Expressions for the equivalent velocity and damping of a rock mass are derived herein for the case of long-wavelength propagation normal to the plane of joints. The shear displacement,  $\delta_{\text{mass}}$ , experienced by a rock-joint repetitive unit combines the displacement in the intact rock,  $\delta_r$ , and in the joint,  $\delta_j$  (Fig. 2):

$$\delta_{\text{mass}} = \delta_r + \delta_j \quad (8)$$

The displacement can be written in terms of the length of the medium,  $L$ , and the strain,  $\delta = L\gamma$ . Furthermore, the strain reflects the applied shear stress,  $\tau$ , and the stiffness,  $G$ , of the medium,  $\gamma = \tau/G$ , and the stiffness is related to the wave velocity,  $V$ , and the mass density,  $\rho$ ,  $G = V^2\rho$ . Replacing these relations into equation (8):

$$\delta_{\text{mass}} = \frac{\tau L_{\text{mass}}}{\rho_{\text{mass}} V_{\text{mass}}^2} = \frac{\tau L_r}{\rho_r V_r^2} + \frac{\tau L_j}{\rho_j V_j^2} \quad (9)$$

The shear stress,  $\tau$ , is the same in the gouge as in the rock block. Therefore the expression for the velocity in the rock mass becomes

$$V_{\text{mass}}^{(\text{long } \lambda)} = \sqrt{\frac{1}{\frac{1 - \eta \rho_{\text{mass}}}{V_r^2 \rho_r} + \frac{\eta \rho_{\text{mass}}}{V_j^2 \rho_j}}} \quad (10)$$

where  $\rho_{\text{mass}} = \rho_r(1 - \eta) + \rho_j\eta$ . The expression in equation (10) is known as *Backus' average*.

Long-wavelength propagation,  $\lambda \gg L_{\text{mass}}$ , does not experience reflections at interfaces because the wave travels through the medium as in a continuum without noticing the presence of interfaces. However, losses in the two media contribute to the total loss in the medium. Damping is the ratio between the energy lost,  $\Delta W$ , and the energy stored,  $W$ , per cycle:

$$D_{\text{mass}}^{(\text{long } \lambda)} = \frac{\Delta W}{4\pi W} = \frac{1}{4\pi} \frac{\Delta W_j + \Delta W_r}{W_j + W_r} \quad (11)$$

In each material, the energy lost can be computed in terms of the known damping,  $\Delta W = 4\pi WD$ . The energy stored when a shear force  $F_T$  is applied is  $W = F_T\delta/2$ , where the displacement can be written in terms of the length of the medium,  $L$ , and the strain,  $\delta = L\gamma$ . Finally, the strain reflects the applied shear stress,  $\tau = F_T/A$ , and the stiffness,  $G$ , of the medium,  $\gamma = F_T/GA$ , where  $A$  is the cross-sectional

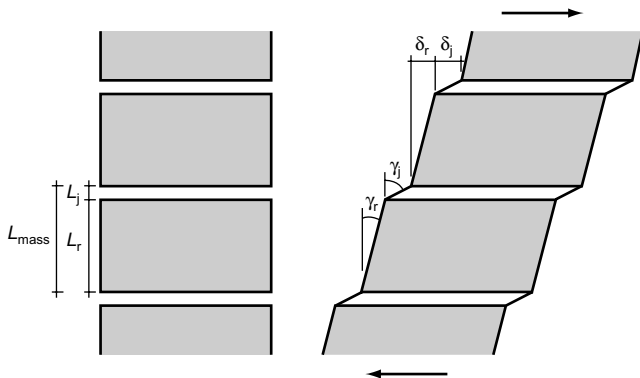


Fig. 2. Long-wavelength propagation: effective shear stiffness in a jointed rock mass

area. Recognising that the same level of shear stress,  $F_T/A$ , is imposed on the rock as on the joint material, the expression for the damping of the rock mass for long-wavelength propagation becomes

$$D_{\text{mass}}^{(\text{long } \lambda)} = \frac{\frac{L_j G_r}{L_r G_j} D_j + D_r}{\frac{L_j G_r}{L_r G_j} + 1} = \frac{\frac{\eta G_r}{1 - \eta G_j} D_j + D_r}{\frac{\eta G_r}{1 - \eta G_j} + 1} \quad (12)$$

If the quantity  $\eta G_r \gg (1 - \eta)G_j$ , then  $D_{\text{mass}}$  is about the same as  $D_j$ ; that is, the damping in the rock mass,  $D_{\text{mass}}$ , is determined by the damping in the joints,  $D_j$ .

#### Intermediate wavelength ( $\lambda \approx L_{\text{mass}}$ )

When the wavelength,  $\lambda$ , approaches the internal scale of the layered medium,  $L_{\text{mass}} = L_r + L_j$ , the wavefront senses the presence of the repetitive jointed rock structure, and the group velocity of the rock mass decreases. In the simplest form, the dispersion relation can be obtained for a sequence of masses and springs connected in series (Brillouin, 1946):

$$V_{\text{mass}}^{(\text{inter } \lambda)} = V_{\text{mass}}^{(\text{long } \lambda)} \cos\left(\frac{\pi L_{\text{mass}}}{\lambda}\right) \quad (13)$$

where  $V_{\text{mass}}^{(\text{inter } \lambda)}$  is the group velocity in the rock mass. When  $\lambda = 2L_{\text{mass}}$ , the attenuation is maximum, the group velocity is zero, and the rock mass acts as a low-pass filter equation (13); see also Morlet *et al.*, (1982).

#### Wave propagation in soil-type gouge

The dynamic properties of the gouge in open joints can be modelled as a soil, in either short-, intermediate-, or long-wavelength propagation models. Micromechanical and experimental relations show that the shear wave velocity at the joint,  $V_j$ , is a power function of the mean stress on the polarisation plane. For a shear wave propagating normal to the plane of the joint (Hardin & Richart, 1963; Lee & Stokoe, 1986; review in Santamarina *et al.*, 2001)

$$V_j = \alpha \left( \frac{1 + K_o \sigma'_n}{2 p_r} \right)^\beta \quad (14)$$

where  $\sigma'_n$  is the effective stress normal to the joint,  $K_o$  is the coefficient of earth pressure at rest under zero lateral strain conditions,  $p_r = 1$  kPa is a reference pressure that renders the equation dimensionally homogeneous, and the parameters  $\alpha$  and  $\beta$  depend on the type of soil. In preloaded soils the equation is modified to take into consideration the stiffening effects of preloading (Viggiani & Atkinson, 1995). The exponent is  $\beta = 1/6$  for spherical Hertzian contacts,  $\beta \approx 0.25$  for medium dense sands, and  $\beta = 0.27-0.45$  for soft clays. Likewise, semi-empirical relations for damping in soils capture the effect of the applied stress (see for example Hardin, 1965):

$$D = \theta \cdot \left( \frac{\sigma'_n}{p_r} \right)^{-\psi} \quad (15)$$

The parameters  $\theta$  and  $\psi$  depend on the soil type and moisture conditions. Both wave velocity and damping are strain independent at small strains, that is, when the propagating wave causes a strain,  $\gamma$ , lower than the linear threshold strain of the soil,  $\gamma_{lt}$ . The linear threshold strain is greater than  $10^{-5}$  for most soils (Vucetic, 1994). As for other granular media, the velocity and attenuation in the gouge depend not only on the state of stress, but also on the degree of saturation, weathering, diagenesis and cementation effects.

### EXPERIMENTAL STUDY: DEVICE, PROCEDURE AND DATA REDUCTION

Shear wave propagation is particularly advantageous in the study of discrete media such as jointed rock masses at low confinement because the shear wave velocity is controlled by the shear stiffness of the medium, and is not affected by the bulk stiffness of the water. Furthermore, shear wave propagation parameters are not affected by geometric dispersion, so that measurements conducted in a rod specimen are directly applicable to the propagation of plane waves in the field (Kolsky, 1963). Hence this study involves the torsional excitation of a columnar specimen made of discrete elements and subjected to axial load, that is, normal to the plane of joints.

The column is designed as a free-fixed dynamic system. Annular discs of the selected material are stacked on a large steel base, which acts as the fixed boundary (Fig. 3). In order to allow a free-end condition at the top end, a 5 mm thick aluminium cap is placed on top of the stack, and the

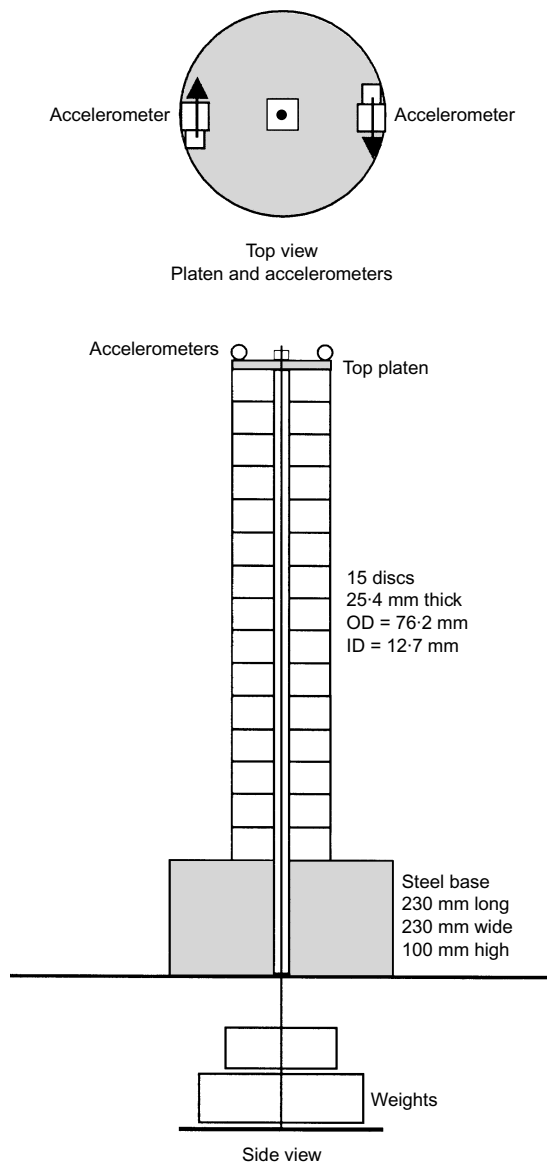


Fig. 3. Sketch of the device for wave propagation studies in jointed media. The normal stress is applied with weights hanging on the central rod, which is anchored at the top platen. Accelerometers are placed at diametrically opposed locations and aligned in a clockwise direction

axial load is hung from the aluminium cap by means of a thin rod that runs along the centre hole in the discs. The upper end of the loading rod is anchored to the top cap, and weights are hung at the lower end of the rod (Fig. 3). Because the loading rod runs along the centre of the column, it does not affect the torsional vibration response (Stokoe *et al.*, 1985; Santamarina & Cascante, 1996). For a given specimen, wave propagation measurements are conducted at different axial loads, during both loading and unloading paths.

The wavelength in the first-mode torsional vibration in a fixed-free system is four times the length of the column. Therefore, if the column is made of  $n$  discs and the inter-joint spacing is  $L_{\text{mass}}$ , the wavelength in the first-mode vibration is  $\lambda = 4nL_{\text{mass}}$ . The value of  $n$  is selected so that long-wavelength propagation is attained ( $\lambda \gg L_{\text{mass}}$ ), and dispersion effects related to the discrete nature of the column are avoided (equation (13)). Very slender columns tend to promote strong flexural motion, and the signal-to-noise ratio decays for the torsional response. A 15-disc column provides strong torsional signals, and the error in velocity due to Brillouin dispersion is less than  $10^{-6}$ .

The torsional excitation is created by suddenly releasing the column from a quasi-static rotation enforced at the top of the column, allowing it to vibrate freely. This source is implemented by applying a minute torque at the centre of the cap with a brittle 0.5 mm pencil lead. The fracture of the lead releases the column, that is, a step function from the initial imposed deformation. This type of source replaces the standard magnet coil system in resonant columns, and avoids measurement difficulties and damping bias related to the counter-electromotive force. All measurements are conducted at a global strain  $\gamma_{\text{mass}} < 10^{-5}$ .

Two accelerometers are used to monitor the torsional vibration of the column. They are mounted on the top aluminium cap at diametrically opposite locations; their axes are aligned normal to the radius of the column, and both are directed in a clockwise direction, as shown in Fig. 3. The signals are anti-alias filtered, digitised with a digital storage oscilloscope, and stored for post-processing.

#### Data reduction: velocity and damping

The processing of the accelerometer signatures involves time- and frequency-domain operations. Frequency-domain operations are made possible by the linear and time-invariant material response at small strains and within the short duration of the excitation, which is always  $< 1$  ms. The analytical signal method was used to compute instantaneous parameters and to corroborate global results.

The first signal processing operation is implemented in the time domain and involves adding the signals obtained with the two accelerometers. Signal addition enhances the torsional response and minimises the flexural response in the combined signal, as shown in Fig. 4.

The combined signal is then transformed to the frequency domain. Because the flexural and torsional resonant frequencies are very different in this column, there is no modal superposition and a clear torsional resonance is observed. The measured torsional spectral response is fitted with the theoretical response of a single-degree-of-freedom system to obtain the resonant frequency,  $f_n$ , and the rock mass damping,  $D_{\text{mass}}^{(\text{long } \lambda)}$  (Fig. 5):

$$|H(f)| = \frac{1}{\left| 1 + j2D_{\text{mass}}^{(\text{long } \lambda)} \frac{f}{f_n} - \left( \frac{f}{f_n} \right)^2 \right|} \quad (16)$$

The velocity,  $V_{\text{mass}}^{(\text{long } \lambda)}$ , is computed from the resonant fre-

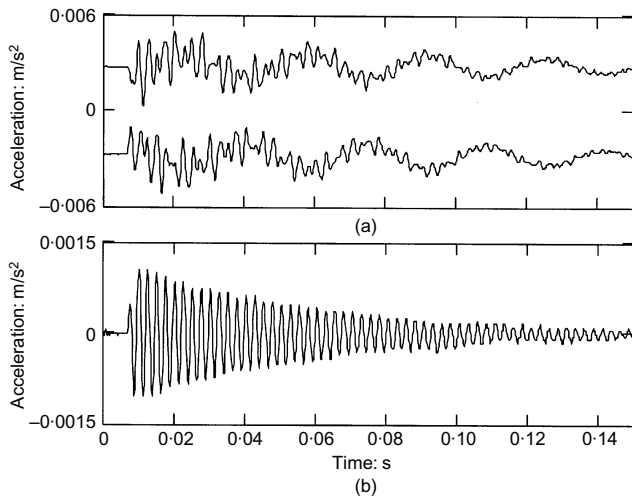


**Fig. 4.** Time series captured with the two accelerometers for the specimen with clean joints subjected to 75 kPa normal stress. (a) The high-frequency torsional response rides over the lower frequency flexural response. The low-frequency flexural responses are out of phase because both accelerometers are aligned in the clockwise direction. (b) The flexural component is largely cancelled by adding the two time series

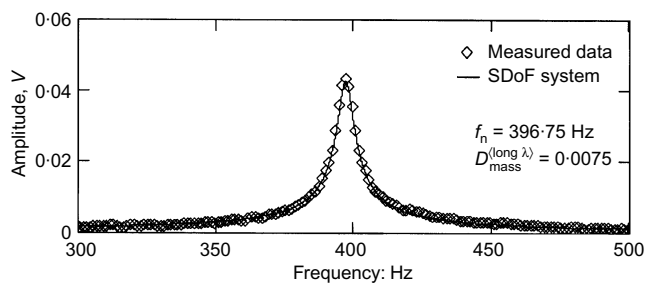


**Fig. 5.** Frequency response in torsional mode. The natural frequency,  $f_n$ , and the damping,  $D_{\text{mass}}^{(\text{long } \lambda)}$ , are obtained by fitting the single-degree-of-freedom system response (equation (16)) to the data

quency,  $f_n$ , assuming a wavelength four times the length,  $L$ , of the free-fixed column:

$$V_{\text{mass}}^{(\text{long } \lambda)} = 4Lf_n \quad (17)$$

The data reduction methodology described above permits the attainment of high accuracy in velocity ( $\pm 0.25\%$ ) and in damping (about  $\pm 5\%$ , even for damping values as low as  $D = 0.007$ ). The implementation of these signal processing procedures is outlined in Santamarina & Fratta (1998).

## RESULTS

The discs used in this study resemble sandstone, and are commercially available grinding wheels. Kaolinite clay was placed in between the discs to simulate the presence of gouge. A summary of the physical and chemical characteristics of the discs and the clay is presented in Table 1.

Several specimens were prepared and tested by varying the thickness of the clay layer between discs. The complete dataset can be found in Fratta (1999). Table 2 presents a summary of the geometric characteristics for the tested specimens.

**Table 1.** Properties of selected materials

Discs: grinding wheels (Norton, Worcester, MA)	
Composition	Grains: aluminium oxide (medium hardness) Grit size: 60 Bond: glass fibre
Dimensions	Thickness, $L_r = 25.4$ mm Inside diameter = 12.7 mm Outside diameter = 76.2 mm
Mass density	$\rho = 2300$ kg/m <sup>3</sup>
Air-dry moisture content	$w = 0.3\%$
Wave velocity	$V_P = 3735$ m/s $V_S = 2015$ m/s
Gouge material: kaolinite (Wilkinson Kaolin Associates, Gordon, GA)	
Mean particle diameter	$D_{50} = 3.6 \times 10^{-7}$ m
Specific surface	$S_s = 21.9$ m <sup>2</sup> /g
Specific gravity	$G_s = 2.6$
Air-dry moisture content	$w = 1\%$

**Table 2.** Properties of tested specimens

Nominal joint thickness	Joint condition and joint ratio, $\eta$
0.0 mm	Clean interfaces Initial height of the column = 388 mm Final height of the column = 387.75 mm Joint ratio, $\eta = 0.019$
0.5 mm	Filled with 0.5 mm kaolinite Initial height of the column = 395 mm Final height of the column = 393.25 mm Joint ratio, $\eta = 0.035$
1.0 mm	Filled with 1.0 mm kaolinite Initial height of the column = 399.5 mm Final height of the column = 397 mm Joint ratio, $\eta = 0.047$
2.0 mm	Filled with 2.0 mm kaolinite Initial height of the column = 411 mm Final height of the column = 406.5 mm Joint ratio, $\eta = 0.072$
2.5 mm	Filled with 2.5 mm kaolinite Initial height of the column = 415 mm Final height of the column = 410 mm Joint ratio $\eta = 0.082$

## Experimental results and observations

Figures 6–10 present the change in wave velocity and damping for each specimen during loading and unloading paths, with respect to the applied normal stress. The following observations can be made:

- The shear wave velocity increases with increasing normal stress. This trend is observed in all specimens.
- The shear wave velocity is higher during unloading in all specimens with clay in the joints, but there is no preloading effect on the specimen with clean joints. This result suggests that preloading stiffening is happening primarily in the clayey gouge. This is a typical soil response, particularly when preloading takes place at zero lateral strain, which is the case for the clay in the joints.
- At all stress levels, the shear wave velocity decreases as the gouge thickness increases, as highlighted in the summary plot in Fig. 11(a). Therefore the impact of the kaolinite on the global wave velocity increases as

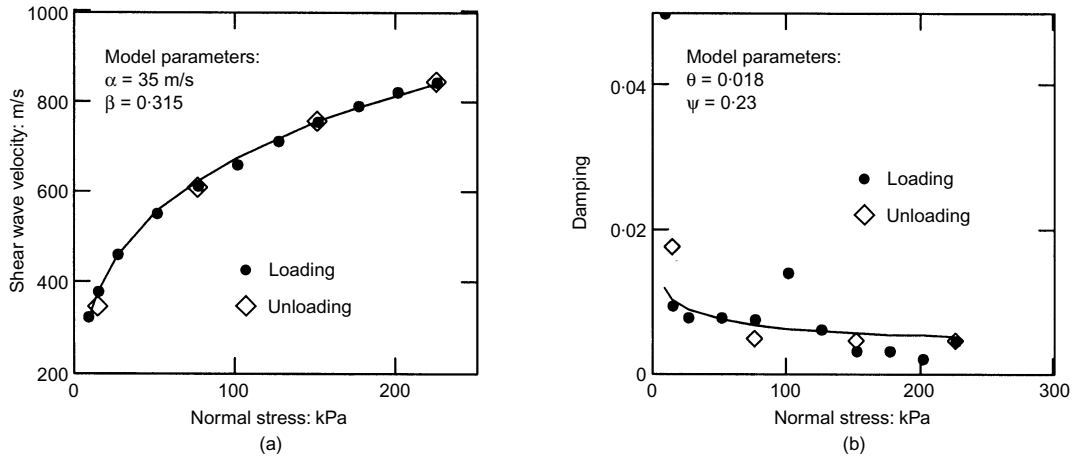


Fig. 6. Specimen without gouge (0.0 mm): (a) shear wave velocity against normal stress; (b) damping against normal stress. Velocity and damping data are fitted using the models in equations (10) and (12). The stress-dependent behaviour of the gouge is modelled using the empirical relations in equations (14) and (15)

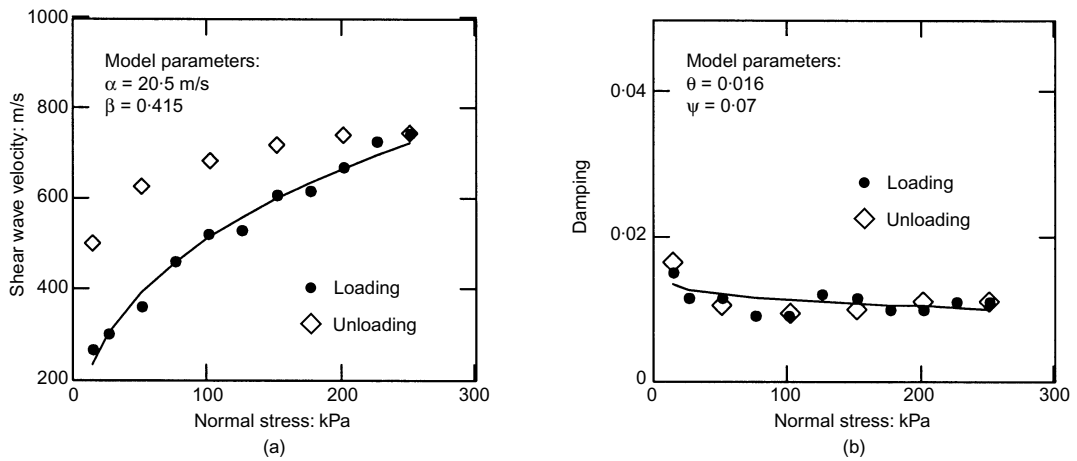


Fig. 7. Specimen 0.5 mm kaolinite gouge: (a) shear wave velocity against normal stress; (b) damping against normal stress. Velocity and damping data are fitted using the models in equations (10) and (12). The stress-dependent behaviour of the gouge is modelled using the empirical relations in equations (14) and (15)

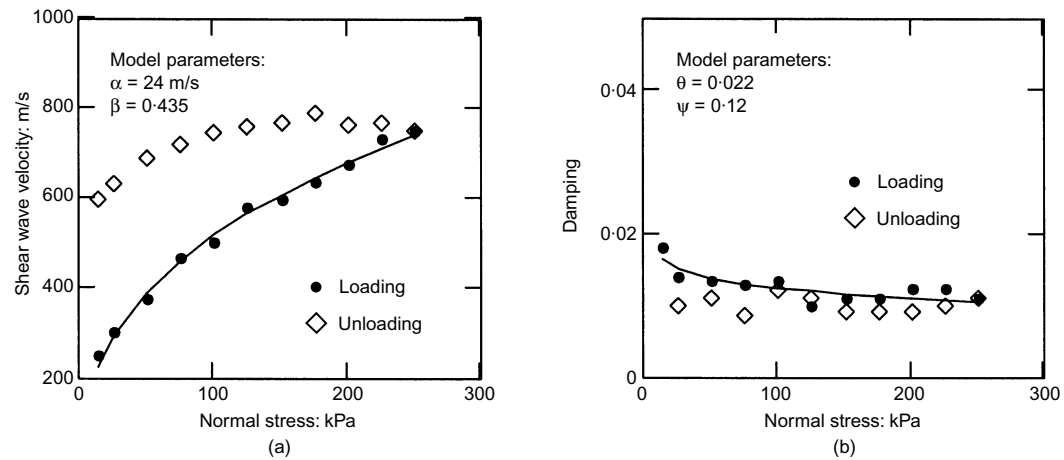


Fig. 8. Specimen 1.0 mm kaolinite gouge: (a) shear wave velocity against normal stress; (b) damping against normal stress. Velocity and damping data are fitted using the models in equations (10) and (12). The stress-dependent behaviour of the gouge is modelled using the empirical relations in equations (14) and (15)

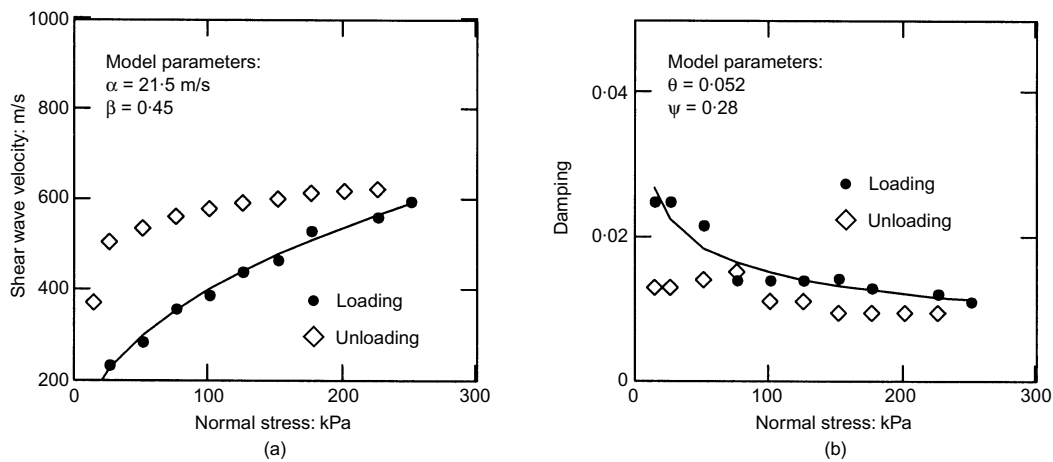


Fig. 9. Specimen 2.0 mm kaolinite gouge: (a) shear wave velocity against normal stress; (b) damping against normal stress. Velocity and damping data are fitted using the models in equations (10) and (12). The stress-dependent behaviour of the gouge is modelled using the empirical relations in equations (14) and (15)

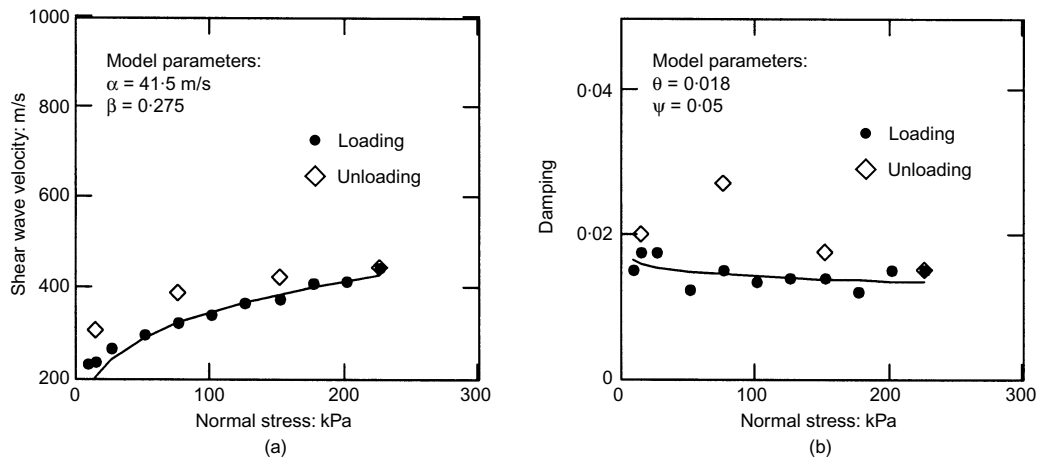


Fig. 10. Specimen 2.5 mm kaolinite gouge: (a) shear wave velocity against normal stress; (b) damping against normal stress. Velocity and damping data are fitted using the models in equations (10) and (12). The stress-dependent behaviour of the gouge is modelled using the empirical relations in equations (14) and (15)

the joint ratio,  $\eta$ , increases, in agreement with equation (10).

- (d) Damping data exhibit more variability than shear wave velocity data.
- (e) Damping values tend to decrease as the normal stress increases. Such a response is also observed in dry particulate media when damping is the result of thermoelastic relaxation and/or frictional loss (strain above the linear threshold strain), and in moist soils when damping reflects the relative fluid–skeleton mobility.
- (f) As the gouge thickness increases, damping also increases. The correlation is not strong. However, there is a clear distinction between the damping in the specimen with clean joints (no gouge) and all the other specimens, as observed in the summary in Fig. 11(b). Hence the presence of clay in joints adds significant loss to wave propagation.

#### Analyses

Long-wavelength propagation models for velocity and damping are fitted to the data, and plotted as lines in Figs 6–10. In these plots the material properties that capture the joint behaviour,  $V_j$  and  $D_j$ , are replaced by the semi-empirical soil response, equations (14) and (15). Most parameters in the models are independently determined a priori (see Tables 1 and 2), except for the soil parameters  $\alpha$ ,  $\beta$ ,  $\theta$  and  $\psi$  in equations (14) and (15), which are obtained by fitting the data. The intact rock damping is assumed to be  $D_r = 0.0025$ , which corresponds to typical values of damping in sandstone rocks (Carmichael, 1989). For clarity, Figs 6–10 present only the fitting for data gathered during loading. The fitted parameters are shown in the corresponding figures.

When the shear wave velocity is plotted against stress in log–log scales, the clean joint specimen exhibits a single trend (Fig. 12(a)). However, a bilinear trend is found for

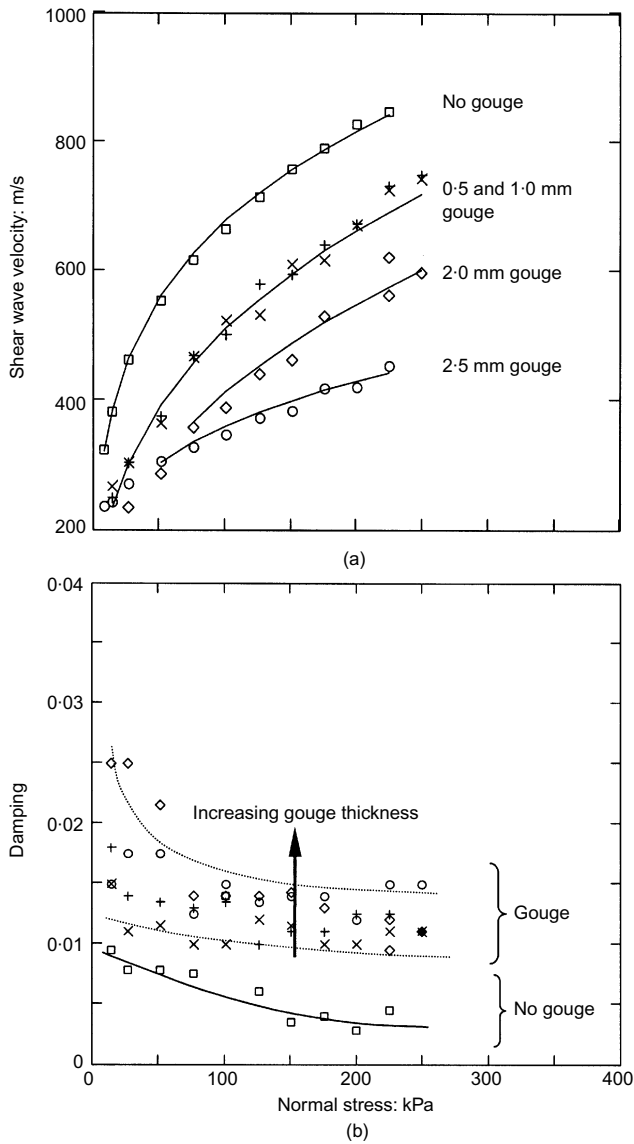


Fig. 11. Summary plots for long-wavelength propagation: (a) shear wave velocity; (b) damping against normal effective stress and gouge thickness

other specimens, as shown in Fig. 12(b). Similar bilinear  $\log V - \log \sigma'_v$  trends are observed in other experimental studies with particulate media (Cascante & Santamarina, 1996; Santamarina & Aloufi, 1999). In those cases, the bilinear trends are associated with important changes in contact behaviour or in fabric within the medium. It is hypothesised that, in the case of these jointed rock specimens, the stiffness of the kaolinite gouge determines the wave velocity at low stresses; however, as the normal stress increases, the joint aperture reduces and neighbouring blocks come into contact. In general, the nature of joint stiffness will change from asperity-gouge-asperity to direct asperity-asperity contact between blocks when the thickness of gouge approaches the height of asperities.

DISCUSSION

Soil or jointed rock?

Published results and those results presented here suggest that elastic wave propagation studies can render information related to

- (a) soil-rock distinction and characterisation
- (b) assessment of preferential joint alignment and anisotropy (Pyrak-Nolte *et al.*, 1990a, 1990b; Santamarina & Cascante, 1996).
- (c) evaluation of the state of stress from relations such as equation (14). This can be further extended into tomographic imaging of the evolution of the state of stress, for example in reference to foundations, tunnels and slopes (reviewed in Santamarina & Fratta, 1998)
- (d) characterisation of the joint spacing from the spectral response, as the wavelength approaches the joint spacing (equation (13); Pyrak-Nolte *et al.*, 1990a, 1990b).

The first observation requires further analysis. The question guiding this discussion is whether the engineer, not knowing that the medium is a jointed rock mass, could justify the data by assuming a soil model. To address this question, the soil model in equation (14) is fitted to the velocity-stress measurements gathered with the different specimens, and compared with the fitting attained with the mixed rock-soil model (equation (10) Figs 6-10). Very similar-quality fitting is obtained using either model—that is, similar residual error—even though the two models are based on very different assumptions about the medium.

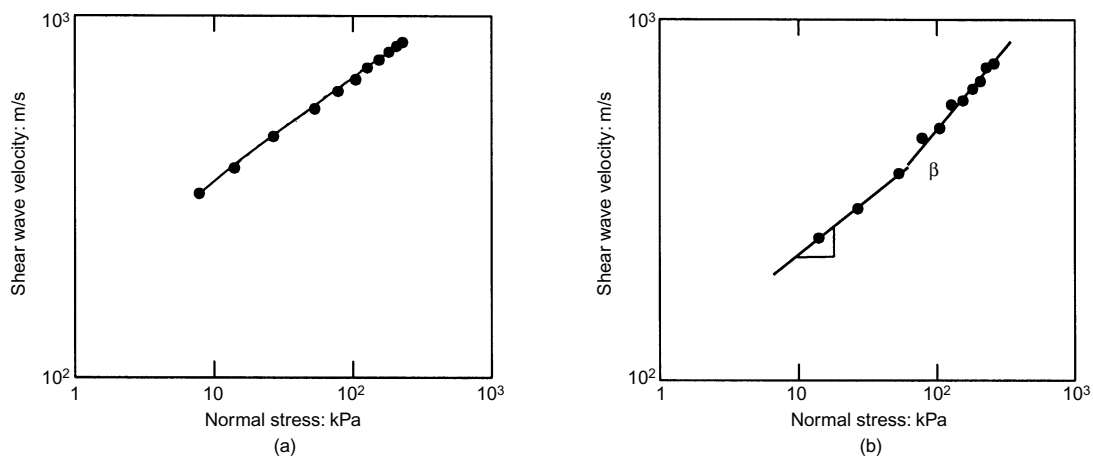


Fig. 12. Shear wave velocity against normal stress for the column with: (a) no gouge; (b) 1 mm gouge. The slope,  $\beta$ , changes with increasing normal stresses in the specimen with gouge at the joint

This result should not lead to the conclusion that the medium cannot be properly identified. The derived  $\alpha$  and  $\beta$  parameters for the jointed rock specimens are compared with parameters obtained for a wide range of particulate materials in Fig. 13. Clearly, distinct trends are observed for soils and for the synthetic jointed rock specimens. Hence soils and jointed rocks can be distinguished on the basis of shear wave velocity data.

There is a pronounced shift in data points between soil specimens and the jointed rock data shown in Fig. 13. The manipulation of equation (10) permits computation of the values of  $\alpha$  and  $\beta$  that would be required to fit the jointed rock data with the soil-type power relation (equation (14)),

$$\alpha_{\text{mass}} = \sqrt{\frac{1}{\frac{1-\eta}{V_r^2} \frac{\rho_{\text{mass}}}{\rho_r} + \frac{\eta}{\alpha^2} \frac{\rho_{\text{mass}}}{\rho_j}}} \approx \sqrt{\frac{\rho_j}{\rho_{\text{mass}}} \frac{1}{\eta}} \alpha \quad (18)$$

$$\beta_{\text{mass}} = \frac{1}{\left[1 + \frac{1-\eta}{\eta} \cdot \frac{\rho_j}{\rho_r} \cdot \left(\frac{V_j}{V_r}\right)^2\right]} \beta \quad (19)$$

Equation (18) predicts a significant increase in the value of  $\alpha$ , in agreement with the observed shift in Fig. 14. On the other hand, while equation (19) predicts that the value of  $\beta$  for the rock mass will be similar to or slightly smaller than that for the soil, experimental results suggest otherwise:  $\beta$  for kaolinite is  $\beta \approx 0.28$ , but the value for the rock mass with joint thickness 0.5, 1.0 and 2.0 mm varies between 0.45 and 0.48. Once again, these results highlight the relevance of a changing mechanism in contact stiffness discussed earlier in reference to Fig. 12.

*Short- and long-wavelength propagation*

Velocity and damping relations for long- and short-wavelength propagation are plotted in Fig. 14. The contribution of the transmission coefficient,  $T$ , to the rock mass damping,  $D_{\text{mass}}$ , in short-wavelength propagation (third term in equation (5)) is frequency dependent. To facilitate the comparison of damping data, this term is not considered in Fig. 14:

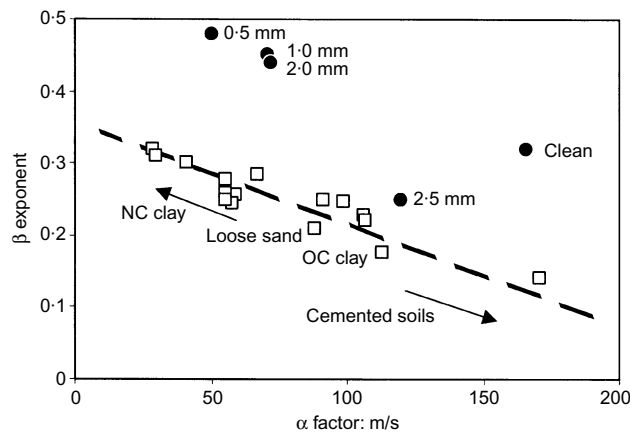


**Fig. 13. Parameters for the velocity–stress power relation (after Fernandez, 2000).** Data shown as open squares were gathered with a wide range of soils; the regression line  $\beta = 0.36 - \alpha/700$  applies to these data, where  $\alpha$  is in m/s. The filled circles represent the  $\alpha$ – $\beta$  values obtained by fitting the jointed rock mass data with the same power relation; the numbers near the dots indicate the gouge thickness. The jointed rock response approaches soil response when the gouge is thick

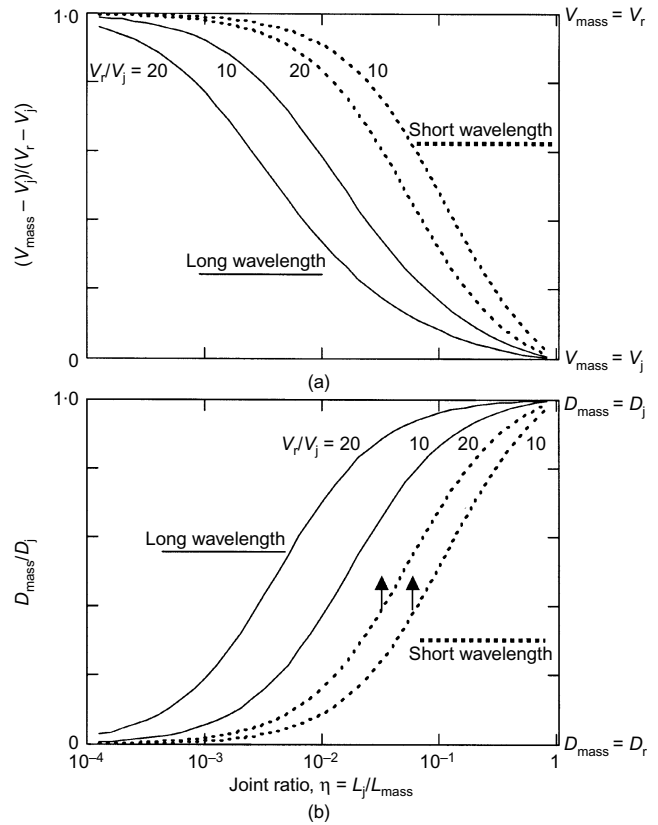


**Fig. 14. Short-wavelength and long-wavelength model predictions: (a) velocity; (b) damping.** The assumed parameters are:  $\rho_r/\rho_j = 1.6$ ;  $D_j \gg D_r$ . The short-wavelength values for rock mass damping do not take into consideration partial transmission effects, i.e.  $T = 1.0$ . Therefore the effective rock mass damping is higher than the plotted values

therefore the values of damping shown for short-wavelength propagation are lower bounds. The following observations can be made:

- (a) In agreement with experimental results (Fig. 11), both models show that velocity decreases and damping increases with increasing gouge thickness, that is, higher joint ratio,  $\eta$ .
- (b) The long-wavelength propagation velocity is more severely affected by the presence of soft joints than the short-wavelength propagation velocity.
- (c) Both short- and long-wavelength models show that velocity decreases and damping increases with softer joints, that is, higher  $V_r/V_j$  ratio.
- (d) Overall, these models predict that velocity will increase as the frequency increases, from the long-wavelength propagation velocity at low frequencies (say,  $\lambda/L_{\text{mass}} > \sim 10$ ), to the short-wavelength propagation velocity at high frequencies (say,  $\lambda/L_{\text{mass}} < \sim 1/10$ ). Attenuation is maximum when  $\lambda \sim 2L_{\text{mass}}$ .

There is an additional important effect of the velocity ratio,  $V_r/V_j$ . The strain levels caused in the gouge,  $\gamma_j$ , and in the rock block,  $\gamma_r$ , are related by

$$\frac{\gamma_j}{\gamma_r} = \frac{G_r}{G_j} = \frac{V_r^2 \rho_r}{V_j^2 \rho_j} \quad (20)$$

Consequently, the strain level experienced in the soil,  $\gamma_j$ , can be significantly higher than in the rock block,  $\gamma_r$ . Furthermore, assuming that the rock stiffness is much greater than the joint stiffness,  $G_r \gg G_j$ , the strain level in the gouge,  $\gamma_j$ ,

is related to the average strain level in the rock mass,  $\gamma_{\text{mass}}$ , by the joint ratio,  $\eta$ :

$$\gamma_j = \frac{\gamma_{\text{mass}}}{\eta} \quad (21)$$

As the strain level in the gouge,  $\gamma_j$ , approaches and exceeds the elastic threshold strain in the soil,  $\gamma_{\text{lt}}$ , the gouge softens ( $G_j$  decreases) and the value of  $D_j$  increases with the strain level. Given the relevance of  $D_j$  to the global rock mass damping (equation (12)), adequate values of damping must be selected. Strain localisation at joints and increased damping may diminish site amplification in a jointed rock mass subsurface.

## CONCLUSIONS

A unique experimental methodology was developed to study long-wavelength propagation in a jointed rock mass, with and without gouge, subjected to low confinement levels relevant to near-surface engineering applications. The device avoids experimental biases, such as the counter-electromotive effect on damping, and permits high-accuracy measurements ( $\pm 0.25\%$  in velocity, and about  $\pm 5\%$  in damping values even for damping as small as  $D = 0.007$ ).

The shear wave velocity increases and the damping ratio decreases with an increase in normal stress. On the other hand, the velocity decreases and the damping increases with increasing gouge thickness. In particular, the presence of clay in joints adds significant loss to wave propagation.

If the semi-empirical velocity–stress power relation  $V = \alpha(\sigma'/\text{pr})^\beta$  is fitted to experimental data gathered for a jointed rock mass, the value of  $\alpha$  corresponding to the jointed rock mass,  $\alpha_{\text{mass}}$ , is much greater than the value for the gouge material,  $\alpha_j$ . Both values are related through the joint ratio,  $\eta$ , as  $\alpha_j \approx \alpha_{\text{mass}}\eta^{-0.5}$ .

When the thickness of gouge approaches the height of rock asperities, there is a gradual change in contact behaviour, from asperity–soil–asperity to asperity–asperity. During this transition the sensitivity of the velocity to the state of stress is highest, and the exponent  $\beta$  in the velocity–stress power relation is high.

The strain localises at joints, and may magnify the displacement-dependent losses. The jointed rock mass acts as a low-pass filter.

The proposed methodology and findings can be used to interpret wave propagation data for rock mass characterisation in the near-surface, and for process monitoring in relation to engineering projects such as excavations and foundations.

## ACKNOWLEDGEMENTS

This research was conducted by the authors at the Georgia Institute of Technology. Support was provided by the National Science Foundation and the Georgia Institute of Technology. Shaun Green helped in evaluating the experimental methodology.

## NOTATION

$A$	cross-sectional area
$D_{50}$	mean particle diameter
$D$	damping
$f$	frequency
$F_T$	shear force
$G$	shear stiffness
$H(f)$	spectral response of a single-degree-of-freedom system
$i$	complex operator
$K_0$	coefficient of earth pressure at rest
$L$	length

$n$	number of discs
$\text{pr}$	reference pressure
$S_s$	specific surface
$T$	reflection coefficient
$t$	travel time in the aperture of the joint
$V$	wave velocity
$w$	gravimetric moisture content
$W$	energy stored
$\Delta W$	energy lost
$Z$	mechanical impedance
$\alpha$	constant in velocity–stress power relation
$\beta$	exponent in velocity–stress power relation
$\gamma$	shear strain
$\delta$	shear displacement in the rock
$\eta$	joint ratio ( $\eta = L_j/L_{\text{mass}}$ )
$\theta$	constant in damping–stress power relation
$\kappa$	specific stiffness
$\lambda$	wavelength
$\rho$	mass density
$\sigma'_n$	effective stress normal to the joint
$\tau$	shear stress
$\psi$	exponent in damping–stress power relation

## REFERENCES

- Boadu, F. K. & Long, L. T. (1996). Effects of fractures on seismic-wave velocity and attenuation. *Geophys. J. Int.* **127**, 86–110.
- Brekhovskikh, L. (1960). *Waves in layered media*. New York: Academic Press.
- Brillouin, L. (1946). *Wave propagation in periodic structures*. New York: McGraw-Hill.
- Carmichael, R. S. (1989). *CRC practical handbook of physical properties of rocks and minerals*. Boca Raton, FL: CRC Press.
- Cascante, C. G. & Santamarina, J. C. (1996). Interparticle contact behavior and wave propagation. *ASCE J. Geotech. Engng* **122**, 831–839.
- Crampin, S. (1977). A review of the effects of anisotropy layering in the propagation of seismic waves. *Geophys. J. R. Astron. Soc.* **49**, 9–27.
- Crampin, S. (1984). An introduction to wave propagation in anisotropic media. *Geophys. J. R. Astron. Soc.* **76**, 17–28.
- Fernandez, A. L. (2000). *Tomographic imaging the state of stress*. PhD dissertation, Georgia Institute of Technology.
- Fratta, D. (1999). *Passive and active measurements of unique phenomena in geotechnical engineering*. PhD thesis, Georgia Institute of Technology.
- Goodman, R. E. (1989). *Introduction to rock mechanics*, 2nd edn. New York: John Wiley & Sons.
- Guéguen, Y. & Palciauskus, V. (1994). *Introduction to the physics of rock*. Princeton: Princeton University Press.
- Hardin, B. O. (1965). The nature of damping in sands. *J. Soil Mech. Found. Engng* **91**, No. SM1, 63–97.
- Hardin, B. O. & Richart, F. E. (1963). Elastic wave velocity in granular soils. *J. Soil Mech. Found., ASCE* **94**, No. SM2, 352–369.
- Helbig, K. (1984). Anisotropy and dispersion in periodically layered media. *Geophysics* **49**, No. 4, 364–373.
- Jumikis, A. R. (1983). *Rock mechanics*, 2nd edn. Rockport, MA: Trans Tech Publications.
- Kolsky, H. (1963). *Stress waves in solids*. New York: Dover Publications.
- Lee, S. H. H. & Stokoe, K. H. (1986). *Investigation of low amplitude shear wave velocity in anisotropic materials*, Report GR86–06. Civil Engineering Department, University of Texas, Austin.
- Mavko, G., Mukerji, T. & Dvorkin, J. (1998). *The rock physics handbook*. New York: Cambridge University Press.
- Morlet, J., Arens, G., Fourgeau, E. & Giard, D. (1982). Wave propagation and sampling theory. Part I: Complex signals and scattering in multilayered media. *Geophysics* **47**, No. 2, 201–221.
- Postma, G. W. (1955). Wave propagation in a stratified medium. *Geophysics* **20**, No. 4, 780–806.
- Pyrak-Nolte, L. J., Myer, L. R. & Cook, N. G. (1990a). Transmis-

- sion of seismic wave across single natural fractures. *J. Geophys. Res.* **95**, No. B6, 8617–8638.
- Pyrak-Nolte, L. J., Myer, L. R. & Cook, N. G. (1990b). Anisotropy in seismic velocities and amplitudes from multiple parallel fractures. *J. Geophys. Res.* **95**, No. B7, 11345–11358.
- Santamarina, J. C. & Aloufi, M. A. (1999). Small strain stiffness: a micromechanical experimental study. *Proc. 2nd Int. Symp. Pre-Failure Deformation Characteristics of Geomaterials, Torino*, 451–458.
- Santamarina, J. C. & Cascante, J. C. (1996). Stress anisotropy and wave propagation: a micromechanical view. *Can. Geotech. J.* **33**, 770–782.
- Santamarina, J. C. & Fratta, D. (1998). *Introduction to discrete signals and inverse problems in civil engineering*. Reston, VA: ASCE Press.
- Santamarina, J. C., Klein, K. A. & Fam, M. A. (2001). *Soils and waves*. New York: John Wiley & Sons.
- Stokoe, K. H., Lee, S. H. & Knox, D. P. (1985). Shear moduli measurements under true triaxial stresses. In *Advances in the art of testing soils under cyclic conditions* (ed. V. Khosla), pp. 166–185. New York: ASCE.
- Viggiani, G. & Atkinson, J. H. (1995). Stiffness of fine-grained soils at very small strains. *Géotechnique* **45**, No. 2, 249–265.
- Vucetic, M. (1994). Cyclic threshold shear strain in soils. *J. Geotech. Engng, ASCE* **120**, 2208–2228.
- White, J. E. (1983). *Underground sound: Application of seismic waves*. Amsterdam: Elsevier.
- Wyllie, M. R. J., Gregory, A. R. & Gardner, L. W. (1956). Elastic wave velocities in heterogeneous porous media. *Geophysics* **21**, 41–70.